



**HAL**  
open science

## Effect of silver and strontium incorporation route on hydroxyapatite coatings elaborated by rf-SPS

Marine Chambard, Djamel Remache, Yannick Balcaen, Olivier Dalverny, Joël Alexis, Robin Siadous, Reine Bareille, Sylvain Catros, Pascal Fort, David Grossin, et al.

### ► To cite this version:

Marine Chambard, Djamel Remache, Yannick Balcaen, Olivier Dalverny, Joël Alexis, et al.. Effect of silver and strontium incorporation route on hydroxyapatite coatings elaborated by rf-SPS. *Materialia*, 2020, 12, pp.100809. 10.1016/j.mtla.2020.100809 . hal-03218463

**HAL Id: hal-03218463**

**<https://hal.science/hal-03218463>**

Submitted on 5 May 2021

**HAL** is a multi-disciplinary open access archive for the deposit and dissemination of scientific research documents, whether they are published or not. The documents may come from teaching and research institutions in France or abroad, or from public or private research centers.

L'archive ouverte pluridisciplinaire **HAL**, est destinée au dépôt et à la diffusion de documents scientifiques de niveau recherche, publiés ou non, émanant des établissements d'enseignement et de recherche français ou étrangers, des laboratoires publics ou privés.



## Open Archive Toulouse Archive Ouverte





OATAO is an open access repository that collects the work of Toulouse researchers and makes it freely available over the web where possible

This is an author's version published in: <http://oatao.univ-toulouse.fr/27198>

### Official URL:

<https://doi.org/10.1016/j.mtla.2020.100809>

### To cite this version:

Chambard, Marine and Remache, Djamel  and Balcaen, Yannick  and Dalverny, Olivier  and Alexis, Joël  and Siadous, Robin and Bareille, Reine and Catros, Sylvain and Fort, Pascal and Grossin, David and Gitzhofer, François and Bertrand, Ghislaine  
*Effect of silver and strontium incorporation route on hydroxyapatite coatings elaborated by rf-SPS.* (2020) *Materialia*, 12. 1-12. ISSN 25891529

Any correspondence concerning this service should be sent to the repository administrator: [tech-oatao@listes-diff.inp-toulouse.fr](mailto:tech-oatao@listes-diff.inp-toulouse.fr)

# Effect of silver and strontium incorporation route on hydroxyapatite coatings elaborated by rf-SPS

Marine Chambard<sup>a, b, \*</sup>, Djamel Remache<sup>c</sup>, Yannick Balcaen<sup>c</sup>, Olivier Dalverny<sup>c</sup>, Joël Alexis<sup>c</sup>, Robin Siadous<sup>d</sup>, Reine Bareille<sup>d</sup>, Sylvain Catros<sup>d</sup>, Pascal Fort<sup>e</sup>, David Grossin<sup>a</sup>, François Gitzhofer<sup>b</sup>, Ghislaine Bertrand<sup>a</sup>

<sup>a</sup> CIRIMAT, Université de Toulouse, CNRS, INP- ENSIACET 4 allée Emile Monso - BP44362, 31030 Toulouse cedex 4, France

<sup>b</sup> CREPE, Department of Chemical and Biotechnological Engineering, Université de Sherbrooke, Sherbrooke, QC, Canada

<sup>c</sup> LGP, Université de Toulouse, INP/ENIT, 47, avenue d'Azereix, Tarbes, F-65016, France

<sup>d</sup> Inserm, U1026, Tissue Bioengineering, Bordeaux University, Bordeaux, France

<sup>e</sup> PROJECTION PLASMA SYSTEME (2PS), ZI du Colombier, 12220 Montbazens, France

## A B S T R A C T

### Keywords:

rf - Suspension plasma spraying  
doped hydroxyapatite coating  
mechanical properties  
biological properties  
bactericidal properties

Hydroxyapatite coatings have been currently used on hip prostheses for their ability to promote faster osseointegration and bone growth. Nevertheless, post-operative infections remain a recurring problem. To overcome this issue, doping with antibacterial elements has become a new trend. In this work, hydroxyapatite coatings elaborated by radio-frequency suspension plasma spraying (rf-SPS) were doped with silver and strontium. Several doping strategies were explored thanks to the versatility offered by SPS compared with conventional spraying. First way: calcium phosphate doped powders were synthesized by coprecipitation and then dispersed into water before plasma spraying; second way: undoped powder was dispersed into aqueous medium in which nitrates or nanoparticles of the dopant(s) were respectively dissolved/dispersed. XRD revealed a high level of crystallinity ratio (ISO 13 779) and hydroxyapatite proportion for most of the coatings, with the presence of Ag/Ag<sub>2</sub>O nanoparticles whatever the doping route. SEM-EDS and STEM have demonstrated a more homogeneous distribution of the strontium within the coating made from the doped powder. Adherence of the coatings was estimated via a 3-point bending test, while bacteriological tests with *S. aureus* and proliferation of mesenchymal stem cells (hMSC) were performed. The results indicated a preferential incorporation of strontium into the secondary phases, showed efficient bactericidal properties, excellent mechanical properties in comparison with an APS reference coating, and no evidence of cytotoxic effect. This opens the way of a new type of coatings with a finer structure and a higher homogeneity through a better control of physicochemical properties using a suspension as the precursor.

## 1. Introduction

The increase in the world's population and its aging induces an ever-increasing demand for orthopedic prostheses [1]. However, in about 1% of the newly implanted prostheses [2], an infection caused by bacterial agents such as staphylococci or enterobacteria is triggered, requiring new surgery. Such an intervention is both expensive and traumatic. Calcium phosphate coatings have been successfully used for 30 years in orthopaedic surgery since they suppress micro-movements, support bone in-growth and provide osseostability to uncemented hip implants [3,4]. Hydroxyapatite is particularly used as calcium phosphate as it is structurally and chemically similar to bone mineral, and less resorbable than other calcium phosphate phases [5] such as tricalcium phosphate (TCP), tetracalcium phosphate (TTCP), amorphous calcium phosphate (ACP) or

calcium oxide (CaO), whose presence is limited even though typical in plasma-sprayed coating.

The development of hip prostheses which can prevent bacterial infections is therefore a current challenge. The main strategy would consist in adding a doping element with antibacterial and anti-inflammatory properties such as metal elements (Cu, Ag, Zn ...) to hydroxyapatite that is coated on the implant. Among the available dopants, silver is of great interest because of its reactivity with thiolic moieties (especially against gram - bacteria) [6] making it one of the most effective antibacterial agent known at low concentration. Even though first clinical results implying silver doped hydroxyapatite coating are promising [7], a high concentration of silver can be toxic and reportedly causes argyria, hepatopathy, and nephropathy [8,9]. Albers et al. [10] conducted a study in which they demonstrated that the cytotoxicity threshold of silver for osteoblasts and osteoclasts was 2 to 4 times lower than its antibacterial

\* Corresponding author at: CIRIMAT, Université de Toulouse, CNRS, INP- ENSIACET 4 allée Emile Monso - BP44362, 31030 Toulouse cedex 4, France.  
E-mail address: [marine.chambard@ensiacet.fr](mailto:marine.chambard@ensiacet.fr) (M. Chambard).

efficacy against *S. epidermidis*. This same study has also put forward a significant increase in the cytotoxicity of silver particles when their size is reduced from the micro (3  $\mu\text{m}$ ) to the nanometer (50 nm). In parallel, other studies have demonstrated that silver becomes cytotoxic when the concentration in the blood exceeds 2  $\mu\text{g mL}^{-1}$ , but has no adverse effect on hMSC as long as the ionic concentration in the apatite does not exceed 0.7 wt% [11, 12]. In conclusion, many parameters must be considered, and it is necessary to control both the silver concentration in the coating and its release once the prosthesis is implanted. This way, it should be possible to counteract the harmfulness of silver. Fielding et al. showed that strontium, when used in reasonable proportion (3 – 7 at% [13]), can balance the cytotoxicity of silver via osteoblast stimulation and osteoclast inhibition [3, 14], and other would even lend it some antibacterial properties [15]. In addition, Ratnayake et al. [16] reports that silver and strontium-substituted hydroxyapatite has its mechanical properties reinforced, even though its solubility within body fluids increases. Others works confirmed the efficiency and interest of silver and strontium co-doping [17, 18]. This co-doping seems therefore promising for potential clinical applications, even though a special attention shall be given to its impact on the resorption of HA in biological medium, which has been shown to be weakened above a certain substitution degree [16] and determines the sustainability of the device within the body.

Currently, conventional powder plasma spraying (APS) is the technique used by most of the manufacturers to produce coated devices which meet the ISO standards and the FDA requirements [19, 20]. But this technique has its limits. Firstly, because of the use of large powders, it does not allow to reach a microstructure as fine as that of the mineral bone, even though research has highlighted the stimulation of osteoblasts seeded on nanostructured calcium phosphates [21]. And secondly, this technique offers only two ways of integrating these dopants into the coatings: either via the synthesis of a doped powder or by mixing powders of hydroxyapatite and of dopants in oxidized or metallic form [3, 22, 23]. The latter solution leads to a rather poor structural and chemical homogeneity of the coating, and the former has limitation in the chemical composition of the doped powder. Indeed, the synthesis of the silver-doped powder while preserving the stoichiometry of the hydroxyapatite is challenging due to the difference in charge and size of the silver ion  $\text{Ag}^+$ . Typically, silver is only incorporated at a maximum of 10 wt.% [6]. Using a suspension instead of a powder offers an interesting alternative since it allows on one hand spraying smaller (even nanometric) particles leading to finer structures [24], improving the homogeneity of both the coating and the doping, and on the other hand it enriches the doping ways by involving the use of a liquid dispersive medium. In addition, by doping the dispersive medium, a better control of the incorporated amount of dopants while improving their distribution within the coating is expected. The question is: to what extent does the doping protocol used in rf-SPS affect the biological and mechanical properties of the coating?

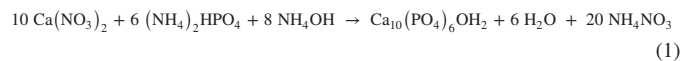
This paper aims to evaluate the mechanical and biological properties of silver and strontium-hydroxyapatite coatings synthesized by rf-SPS, implementing different doping routes. The doping of the suspension was performed either using a powder doped by coprecipitation or dissolving silver and strontium nitrates or adding silver nanoparticles in the dispersive medium. A 3-point bending test was implemented to determine the mechanical adherence of the coatings, while the adhesion and proliferation of hMSC was evaluated to assess their bioactivity, and the development of *staphylococcus aureus* bacteria was tested to establish their bactericidal activity.

## 2. Experimental

### 2.1. Preparation of unsubstituted and Ag/Sr-substituted HA

A pure hydroxyapatite (Hap) powder and another one substituted with Ag and Sr (Ag/Sr-Hap) were synthesized to produce the sus-

pensions destined to rf-SPS plasma spraying. Calcium nitrate tetrahydrate ( $\text{Ca}(\text{NO}_3)_2$ , 4  $\text{H}_2\text{O}$  – Sigma Aldrich), diammonium phosphate ( $(\text{NH}_4)_2\text{HPO}_4$  - Fischer), silver nitrate ( $\text{Ag}(\text{NO}_3)$ , Fischer), strontium nitrate ( $\text{Sr}(\text{NO}_3)_2$ , Sigma-Aldrich) and  $\text{NH}_4\text{OH}$  solution at 20 wt.% (Fischer) were used as chemical precursors for  $\text{Ca}^{2+}$ ,  $\text{PO}_4^{2-}$ ,  $\text{Ag}^+$ ,  $\text{Sr}^{2+}$  and  $\text{OH}^-$ . The unsubstituted calcium phosphate was obtained by coprecipitation according to the following balanced chemical equation (Eq 1):



The powder synthesis protocols were adapted from those described by Kannan [25]. A solution of diammonium phosphate was added to a solution of nitrate(s) such as the Ca/P and (Ca+Sr+Ag)/P ratios of the powders Hap and Ag/Sr-Hap respectively were both set to 1.667 to promote the formation of stoichiometric hydroxyapatite. The pH was maintained at 9 all along the synthesis by adding 20 wt.%  $\text{NH}_4\text{OH}$  to obtain the appropriate acidity of the phosphate ion. The initial molar concentration of the dopants was set to mol.%  $\text{Ag} = \text{Ag}/(\text{Ca}+\text{Sr}+\text{Ag}) = 10.0$  and mol.%  $\text{Sr} = \text{Sr}/(\text{Ca}+\text{Sr}+\text{Ag}) = 5.0$ . After the maturation time (24 h), the powders were filtered and washed with 10 times the reaction medium volume of water before freeze-drying (pressure of 0.10 mbar,  $-80^\circ\text{C}$  for 3 days). The mol% of the dopant within the synthesized powder was measured at 1.41 mol.% for Ag and 5.27 mol.% for Sr. Two powders were synthesized from this protocol, namely Hap and Ag/Sr-Hap.

### 2.2. Suspension preparation

Prior to spraying, the previously described powders (Hap or Ag/Sr-Hap) were dispersed into water at a solid load of 13 wt.%, and an ultrasonic probe was plunged into the suspension for 5 min at 30 W to break up the aggregates, leading up to two suspensions, named after the powders: Hap and Ag/Sr-Hap.

Then, two more Ag and Sr doped suspensions were produced, where the liquid medium was doped instead of the powder: one with silver nanoparticles ( $\text{Ag}^{\text{NP}}$ ), the other one with silver nitrates ( $\text{Ag}^+$ ), and both with strontium nitrates ( $\text{Sr}^{2+}$ ). Undoped Hap was then added to this doped medium, giving rise to two suspensions named  $\text{Hap}+[\text{Ag}^+]/[\text{Sr}^{2+}]$  and  $\text{Hap}+\text{Ag}^{\text{NP}}+[\text{Sr}^{2+}]$ .

In summary, four suspensions were prepared: with the undoped (Hap), with the doped powder (Ag/Sr-Hap), with the undoped powder and nitrates ( $\text{Hap}+[\text{Ag}^+]/[\text{Sr}^{2+}]$ ) and with the undoped powder and a mixture of strontium nitrate and silver nanoparticles ( $\text{Hap}+\text{Ag}^{\text{NP}}+[\text{Sr}^{2+}]$ ), which lead to the synthesis of coatings identified with the same reference as their precursor.

### 2.3. Coatings

#### 2.3.1. Substrates

Titanium alloy Ti-6Al-4 V (grade 5) was selected as the substrate material for its sufficient mechanical strength, anti-corrosion and bioinert properties [26,27]. Plates of  $50 \times 55 \times 1.6 \text{ mm}^3$  adapted to the process were used. The 3-point bending samples ( $50 \times 10 \times 1.6 \text{ mm}^3$ ) were laser pre-cut except at two slots in the titanium plates, as well as cylinders of 10 mm in diameter used for biological and bacteriological tests.

Prior to plasma spraying, the plates were cleaned with solvents (ethanol and acetone in ultrasonic bath) and grit-blasted with alumina (F120) at an incidence angle of  $90^\circ$ , a 120 mm blasting distance and a pressure of 4.5 bar. The arithmetic roughness of the surface (Sa) was determined with a profilometer to be approximately  $1.5 \pm 0.2 \mu\text{m}$ .

#### 2.3.2. Plasma spraying parameters

Rf-SPS coatings were produced at the Université de Sherbrooke (Québec) with a plasma generated by a 50-kW RF plasma torch operating at 3 MHz (PL-50 model from Tekna Plasma System Inc.) equipped

with a supersonic nozzle. The suspension was injected by a peristaltic pump at a feeding rate of 12.5 mL min<sup>-1</sup> and through a supersonic nozzle with a 45 mm output diameter [28]. The liquid atomisation probe was home-designed, and sprays of water droplets with a mean diameter D<sub>50</sub> of 11 μm were produced. The composition of the plasma was a mixture of argon and dioxygen based on previous work performed by Loszach et al. [29], and the generated power was 35 kW, with a pressure within the chamber adjusted to 90 torr. The working distance from the torch to the sample holder was set to 185 mm, and the distance swept by the sample holder under the plasma jet was set to 80 mm. 8 preheating passes followed by 30 spraying passes were necessary to achieve a thickness of about 100 μm.

#### 2.4. Characterization of powders and coatings

All the following characterizations were performed in line with ISO standard (i) ISO 13,779-2:2008 and (ii) ISO 13,779-3:2008 [19, 20].

The particle size distribution was measured with a Malvern Masterizer Hydro 2000S granulometer (UK) in aqueous media, to reproduce the state of the suspension before plasma spraying. The measuring cell was kept under agitation at 1750 rpm for all trials to prevent sedimentation.

The elemental compositions of powders and coatings were measured by an inductively coupled plasma optical emission spectrometer Jobin Yvon Ultima 2 (Horiba, Japan). The roughness of the substrates and the coatings was evaluated using a Sensofar S-Neox confocal microscope (Barcelona, Spain) at x10 magnification. The average value was determined from 5 scanning zones of 1750 × 1300 μm at 0, 90°, 180° and 270°. The crystalline phase analysis of the powders and the coatings were investigated using D8 diffractometer (Bruker AXS GmbH, Karlsruhe, Germany) with Cu Kα radiation (λ = 1.5406 Å) produced at 40 kV and 50 mA. Data were recorded in the 20° - 60° 2θ range with a step size of 0.02° and 38 s per step. The patterns were identified using Match! software and semi-quantitative analyses were realized using the Reference Intensity Ratio method [30], using the following JCPDS data (HA, hydroxyapatite, JCPDS no. 00-009-0432; α-TCP, tricalcium phosphate Ca<sub>3</sub>(PO<sub>4</sub>)<sub>2</sub>, JCPDS no. 04-018-9895; β-TCP, tricalcium phosphate Ca<sub>3</sub>(PO<sub>4</sub>)<sub>2</sub>, JCPDS no. 00-070-2065; TTCP, tetracalcium phosphate, Ca<sub>4</sub>P<sub>2</sub>O<sub>9</sub>, JCPDS no. 00-025-1137; CaO, calcium oxide, JCPDS no. 04-011-9020). The crystallinity ratio R<sub>1</sub> (Eq 2) was calculated according to the formula proposed in the standard ISO 13,779-3, involving the use of a fully crystallised standard (hydroxyapatite powder calcined at 1000 °C for 15 h):

$$R_1 = \frac{\text{Integrated intensity of 10 lines of the sample}}{\text{Integrated intensity of 10 lines of the standard}} \times 100 \quad (2)$$

Fourier Transform Infrared FTIR analysis was carried out with a PerkinElmer 1700 spectrometer (USA) on scraped coatings dispersed in KBr pellets in a ratio of 0.3 percent mass, at a resolution of 4 cm<sup>-1</sup> in the 400 - 4000 cm<sup>-1</sup> range. Chemical state of dopants was evaluated by X-ray photoelectron spectroscopy (XPS) with a VG ESCALAB 220i-XL (ThermoFischer Scientific, US) spectrometer, with a 150 μm-lateral resolution. The observation of surface and microstructure was conducted by SEM with a FEI Quanta450 (Bruker, Germany), using the back-scattering mode at 12.5 kV and 10 mm working distance, and by STEM with a JEM-ARM200F Cold FEG (Jeol, Japan). To determine the porosity from the cross-section images, the samples were cut, then mounted and vacuum impregnated with cold epoxy resin. They were then ground and polished in accordance with the procedure described by Geels et al. [31]. Image analysis were performed with ImageJ on 10 different views, implementing manual thresholding and despeckling. Contact angle measurements were carried out with a Digidrop MCAT goniometer (GBX, Ireland). An equal volume of milliQ water (2 μL) was placed on every sample by means of a micropipette forming a drop on the surface, and the contact angle was recorded 10 s after drop deposition.

#### 2.5. Calcium, silver and strontium release

The evolution of the doped coatings in physiological media and specifically in aggressive medium mimicking the local inflammatory situation appearing after implantation was assessed by implementing dissolution tests in a strong acidic medium. To perform the dissolution test, a cylinder of each specimen except for the Hap+Ag<sup>NP</sup>+ [Sr<sup>2+</sup>] condition was immersed in 50 mL of HNO<sub>3</sub> acidified water at 37 °C, pH 3.5 and subjected to constant shaking in a Dissolutes Sotax CE6 unit (Switzerland) at a 9 mL min<sup>-1</sup> flow rate in closed circulation. An extra coating, synthesized in similar plasma conditions, from a suspension containing a strontium-doped hydroxyapatite powder (3.39 ± 0.04 wt.%) and silver under ionic and metallic form, was annealed at 600 °C for 2 h and tested with the others to highlight the effect of crystallinity on the dissolution behavior of the doped coatings. An aliquot of 10 mL of medium was collected at each time point starting at 30 min, with 10 mL of fresh solution added at each time point, for 5 days. The pH was measured for each aliquot. The aliquot containing the released Ag<sup>+</sup> and Sr<sup>2+</sup> was analysed via atomic absorption spectrophotometer (ContraAA300 Analytik Jena, Germany) for the strontium and calcium, and inductively coupled plasma mass spectrometer (ICP-MS 7500ce, Agilent Technologies, USA) for the silver.

#### 2.6. Mechanical properties

The adherence of a coating is one of the critical characteristics that is required when developing new solutions. The test selected in the present study is a three-point bending test, elaborated by Roche et al. [32] and is described in the ISO 14 679:2001 standard [33]. A polyepoxide stiffener of 25 × 4 × 5 mm<sup>3</sup> is placed and adhered in the center of the surface of the coated test piece, whose surface area is 50 × 10 mm<sup>2</sup>. The whole piece is then placed in an Instron testing machine and is loaded in bending at a crosshead speed of 0.50 mm.min<sup>-1</sup>, until failure. Adhesion energy (mJ) is then calculated from the failure force and the deflection. Then, the residual coating percentage is evaluated with EDS cartography. If the percentage of residual coating is beyond 65%, the rupture is designed as cohesive, below 35% means adhesive, and in between stands for a mixed rupture type. In order to ensure reproducibility of the results, four replicates were used.

#### 2.7. Resazurin assay, cell proliferation

Human mesenchymal stem cells were isolated from human bone marrow aspirates obtained from the University Hospital of Bordeaux after approval by the local ethical commission and written consent of the patient. The Alamar Blue<sup>®</sup> cell viability reagent (ThermoFischer, USA) was used to evaluate cell proliferation. The samples were first placed into an alpha Minimum Essential Medium (α-MEM) (Sigma, USA) for a soaking purpose in 48-well plates. 1 mL of α-MEM + 10% Fetal bovine serum (FBS) holding a density of 50 × 10<sup>3</sup> cells ml<sup>-1</sup> were then seeded onto the samples. At each time point, the medium was withdrawn from the well and 1 mL of α-MEM + 10% serum + 10% alamarBlue solution at 3.5 mg mL<sup>-1</sup> were added. After incubation, 200 μl of the resulting supernatant was transferred to a 96-well plate and read by a plate reader at 590 nm. Cell proliferation was evaluated at 4, 7 and 14 days, and the viability of the cells CV (Eq 3) was estimated through the following formula:

$$CV = \frac{\% \text{proliferation of tested group}}{\% \text{proliferation of reference}} \times 100 \quad (3)$$

For any given experiment, each data point represents the mean ± standard error of five individual cultures. Data were processed by analysis of variance with two-way ANOVA test and Bonferroni's post test to compare all materials with each other at each time. P values < 0.05 were considered to be significant.

**Table 1**  
Physicochemical characteristics of precursors.

	D <sub>10</sub>	D <sub>50</sub>	D <sub>90</sub>	wt.% Ag	wt.% Sr	Ca/P	(Ca+Sr+Ag)/P
Hap	2.8 ± 0.1	9.3 ± 0.3	24 ± 3	–	–	1.68 ± 0.03	–
Ag/Sr-Hap	2.2 ± 0.1	4.6 ± 0.1	9.5 ± 0.2	1.40 ± 0.02	4.30 ± 0.07	1.49 ± 0.03	1.59 ± 0.03
Hap+Ag <sup>NP</sup> +Sr <sup>2+</sup>	2.8 ± 0.1	9.3 ± 0.3	24 ± 3	0.40 ± 0.01	4.37 ± 0.05	1.68 ± 0.03	1.75 ± 0.03
Hap+[Ag <sup>+</sup> ]/[Sr <sup>2+</sup> ]	2.8 ± 0.1	9.3 ± 0.3	24 ± 3	1.54 ± 0.01	4.32 ± 0.02	1.68 ± 0.03	1.77 ± 0.03

## 2.8. Antimicrobial activity

The antimicrobial activity of doped HA-coated samples was determined by challenging with *S. Aureus* (ATCC 33,591, MRSA). The bacterial stock solution was prepared extemporaneously in sterile distilled water before dilution in a culture medium. The prepared samples were sterilized by autoclaving at 121 °C for 15 min and placed into 24-well plates, covered with 2 mL of bacterial suspension 10<sup>3</sup> UFC mL<sup>-1</sup> and incubated by rotation for 24 h at 37 °C. Each sample was taken out at 6, 24 and 48 h and rinsed with 4 mL sterile water and placed into 3 mL of the same solution and shaken by vortex followed by 1 min of ultrasounds. After dilution, 1 mL of the supernatant was seeded in Tryptase Soy Agar (TSA) and the number of visible cells was determined by quantifying CFUs. APS coating was used as a control group; each test was performed in triplicate. The degree of the microbial cell reduction *BR* (Eq 4) was estimated by the following formula:

$$BR = \frac{\sum_{n=3} \text{Log}(\text{Nb bacteria in standard group}) - \sum_{n=3} \text{Log}(\text{Nb bacteria in test group})}{3} \quad (4)$$

## 3. Results

In order to assess the quality of the coatings in respect with the commercial standard, the mechanical and biological tests were also performed with an atmospheric plasma spray (APS) hydroxyapatite standard coating, serving as Reference.

### 3.1. Physico-chemical analysis

#### 3.1.1. Suspension

The suspensions showed very similar characteristics, reported in Table 1. The mean D<sub>50</sub> is comprised between 4.6 ± 0.1 μm for the doped powder and 9.3 ± 0.9 μm for the undoped Hap. Quite similar strontium concentrations of about 4.35 wt.% were determined whatever the doping strategy. 1.40 and 1.54 wt.% were respectively measured for silver in the case of the suspensions formulated either from the doped Ag/Sr-Hap powder or from the undoped Hap powder added with nitrates (Hap+[Ag<sup>+</sup>]/[Sr<sup>2+</sup>]). A lower content of 0.40 wt.% was found for the suspension produced from the undoped powder Hap mixed with Ag<sup>NP</sup> nanoparticles (Hap+Ag<sup>NP</sup>+Sr<sup>2+</sup>). The cation/P ratios vary from 1.68 ± 0.03 for the undoped powder to 1.59 ± 0.02 for the Ag/Sr-doped powder and to 1.76 ± 0.03 for the doped suspensions. XRD patterns of undoped and doped synthesized powders (Fig. 1) show the typical crystallographic apatitic structure of Ca<sub>10</sub>(PO<sub>4</sub>)<sub>6</sub>(OH)<sub>2</sub> (JCPDS 00–009–432), where no secondary crystalline phase is detected. Despite an obvious diminution of the crystallite size, the crystallinity ratio is slightly better for the doped powder with a value of 97 ± 3% for Ag/Sr-Hap, compared with the value of 92 ± 3% for Hap powder.

#### 3.1.2. Coatings

The quantitative XRD analysis (Table 2) establishes that HA is the major phase for all coatings (Fig. 2). 86 wt.% of HA together with a crystallinity ratio of 70% were assessed for the coatings elaborated from Hap undoped powder, with or without doping agents in the suspension. The secondary phases in the doped coatings were TTCP and CaO in quantities twice as large as in the coating produced from the undoped powder that

also contains α-TCP. In contrast, for the coating made with the doped powder Ag/Sr-Hap, an amount of 62 wt.% of HA phase with 33 wt.% of α-TCP were measured, as well as a low crystallinity ratio of 57% in regard to the value recommended in the ISO 13 779–2 standard that must be over 45%. A small peak was noticeable at 2θ = 36° in Ag/Sr-Hap and Hap+[Ag<sup>+</sup>]/[Sr<sup>2+</sup>] patterns, which could be attributed to Ag (JCPDS No. 4–0783) or Ag<sub>2</sub>O (JCPDS no. 19–1155), indicating that the silver ions were possibly turned into metallic or oxidized silver during plasma spraying. FTIR analysis validated the apatite structure of the coatings since all characteristic bands (ν<sub>1</sub> = 938 cm<sup>-1</sup>, ν<sub>2</sub> = 420 cm<sup>-1</sup>, ν<sub>3</sub> = 1017 cm<sup>-1</sup>, and ν<sub>4</sub> = 567 cm<sup>-1</sup>) are present, but also evidenced a diminution of the hydroxylation degree (ν<sub>L</sub>OH<sup>-</sup> = 631 and ν<sub>S</sub>OH<sup>-</sup> = 3570 cm<sup>-1</sup>) for all doped coatings (Fig. 3) [34]. Spectra displayed poorly defined bands that confirmed the poor crystallinity of the Ag/Sr-Hap coating. A weak relative intensity of the bands assigned to OH<sup>-</sup> group evidences a low hydroxylation degree for both Ag/Sr-Hap and Hap+[Ag<sup>+</sup>]/[Sr<sup>2+</sup>] coatings in comparison with the undoped Hap and Hap+Ag<sup>NP</sup>+Sr<sup>2+</sup> coatings. This indicates that silver nanoparticles promote the maintenance of apatite hydroxylation during plasma spraying, probably because they are likely to consume heat in a larger extent through their melting and vaporization steps.

The cross sections of the coatings (Fig. 4) observed by SEM shows a good quality of interface and a uniform microstructure, with some heterogeneous zones and cracks, characteristic of plasma spraying as already mentioned in literature [27]. The porosity evolves from about 3% for Hap+[Ag<sup>+</sup>]/[Sr<sup>2+</sup>] and Hap+Ag<sup>NP</sup>+Sr<sup>2+</sup> coatings to 5% for Ag/Sr-Hap and 7% for the undoped coating Hap. It seems that the presence of nitrates within the suspension diminishes the porosity of the produced coatings. A similar trend can be noticed for the roughness. Indeed, Sa parameters equal to 4.4 ± 0.1 μm were measured for both Hap+[Ag<sup>+</sup>]/[Sr<sup>2+</sup>] and Hap+Ag<sup>NP</sup>+Sr<sup>2+</sup> coatings and higher values of about 5.4 ± 0.4 μm were recorded for both Hap and Ag/Sr-Hap coatings. The presence of silver or silver oxide particles was clearly evidenced into both Ag/Sr-Hap and Hap+[Ag<sup>+</sup>]/[Sr<sup>2+</sup>] microstructures using SEM images at high magnification in backscattering mode (Fig. 5) These nanoparticles were mainly located at the splats-pores borders as shown in Fig. 5b, supporting the hypothesis that silver does not favorably substitute in the apatitic structure. The SEM image analysis of these particles resulted in a mean diameter of 230 ± 95 nm when the doped powder is implemented in the spray system and 115 ± 91 nm when silver is introduced as nitrate in the suspension. But considering the limits of the SEM, even smaller particle sizes around 1.5 μm in diameter could be detected by STEM. Finally, EDS cartography (Fig. 6) performed on the Hap+[Ag<sup>+</sup>]/[Sr<sup>2+</sup>] confirmed the incorporation of strontium to an extent depending on the melting degree of the particle at impact. Indeed, splats showed low variations of strontium content from one to the other, probably due to the implementation process which led to a variable concentration of strontium into hydroxyapatite particles, depending on their size and their melting degree. The EDS mapping performed on the Ag/Sr-Hap coating showed on the other hand a homogenous distribution of strontium (Fig. 6c and 6g) all over the microstructure, confirming its substitution in the apatite.

Elemental quantification of the scraped coatings reveals a loss of the silver content during plasma spraying: 74% loss of the initial silver proportion for the Ag/Sr-Hap coating, 80% for Hap+[Ag<sup>+</sup>]/[Sr<sup>2+</sup>] coating and 85% in the case of Hap+Ag<sup>NP</sup>/Sr<sup>2+</sup> coating (Table 3). The Ca/P

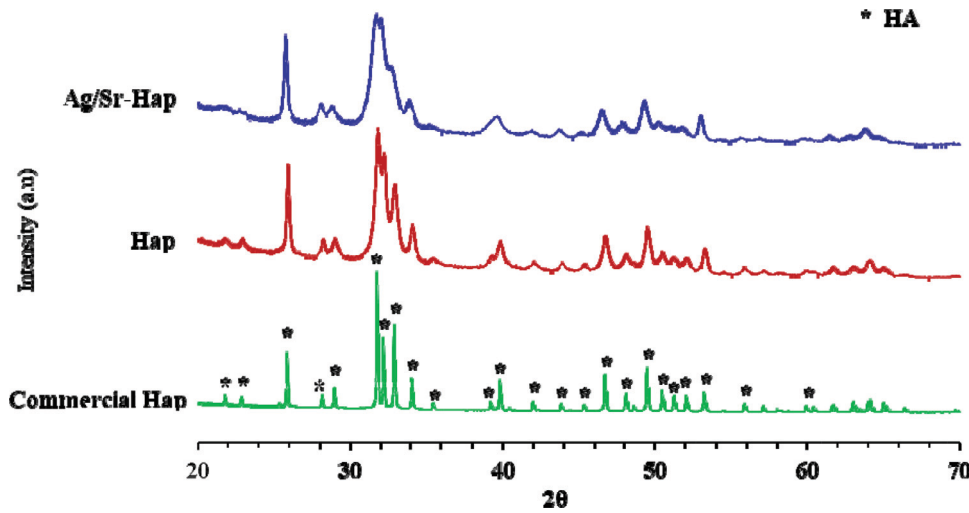


Fig. 1. X-Ray diffractograms of undoped and doped synthesized powders compared with a commercial fully crystallised hydroxyapatite.

Table 2  
Crystallographic composition obtained by RiR method and crystallinity ratio of coatings (ISO 13,779-3 [20]).

	Hap	Ag/Sr-Hap	Hap+[Ag <sup>+</sup> ]/[Sr <sup>2+</sup> ]	Hap+Ag <sup>NP</sup> + [Sr <sup>2+</sup> ]	Annealed doped coating
HA (wt%)	86 ± 4	63 ± 13	83 ± 2	86 ± 5	98
β-TCP (wt%)	-	-	-	-	1.4
α-TCP (wt%)	5.9 ± 1.9	33 ± 11	-	-	-
TTCP (wt%)	7.4 ± 1.6	4.0 ± 2.2	15 ± 2	12 ± 4	-
CaO (wt%)	0.7 ± 0.3	0.1 ± 0.2	1.9 ± 0.6	1.6 ± 0.6	1.0
R <sub>1</sub> (%)	71 ± 5	57 ± 11	68 ± 5	70 ± 4	90
R <sub>p</sub> (%)	5.2	4.6	5.6	5.4	3.2

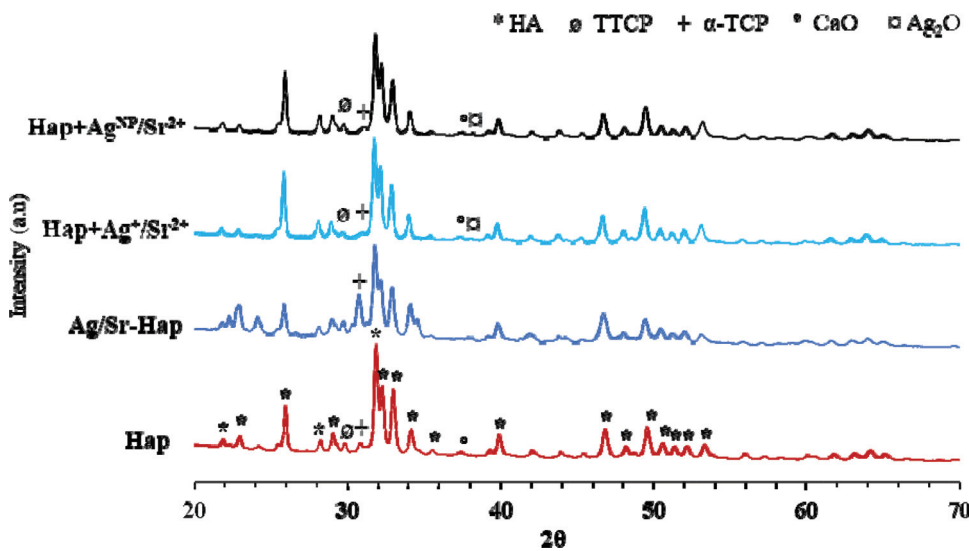


Fig. 2. X-Ray diffractograms of doped and undoped rf-suspension plasma sprayed coatings.

ratio is highly over 1.667 for every coating entailing the undoped powder (Hap, Hap+Ag<sup>NP</sup>+Sr<sup>2+</sup>, Hap+[Ag<sup>+</sup>]/[Sr<sup>2+</sup>]). The one produced from the doped powder is very close to stoichiometry when considering the (Ca+Sr+Ag)/P ratio instead of the Ca/P ratio. Strontium did not suffer any significant loss, since its concentration ranges from 4.24 ± 0.08 to 4.62 ± 0.07 wt.% in the coatings.

The contact angles vary significantly from one coating to the other, as displayed in Table 3. But overall, they all stand below 60° which is considered as the upper threshold to favorize cell attachment according to Yeung et al. [35]. Almost hydrophobic behavior can be assigned to coatings produced from suspensions containing nitrates: 47.6° for

Hap+[Ag<sup>+</sup>]/[Sr<sup>2+</sup>] and 38.8° for Hap+Ag<sup>NP</sup>+Sr<sup>2+</sup>. In contrast coatings produced with the Hap and Ag/Sr-Hap powders are more hydrophilic (17.8° and 22.1° respectively).

### 3.2. Cations release

The kinetics of release of Ca and Sr are reported in Fig. 7a and 7b respectively. Both figures revealed that a large release of Ca and Sr in the acidic medium was noticed during the first 500 min of immersion. After 10 h the concentrations of calcium and strontium leveled off to evolve very slowly up to 4 days. At the end of the assay the disso-

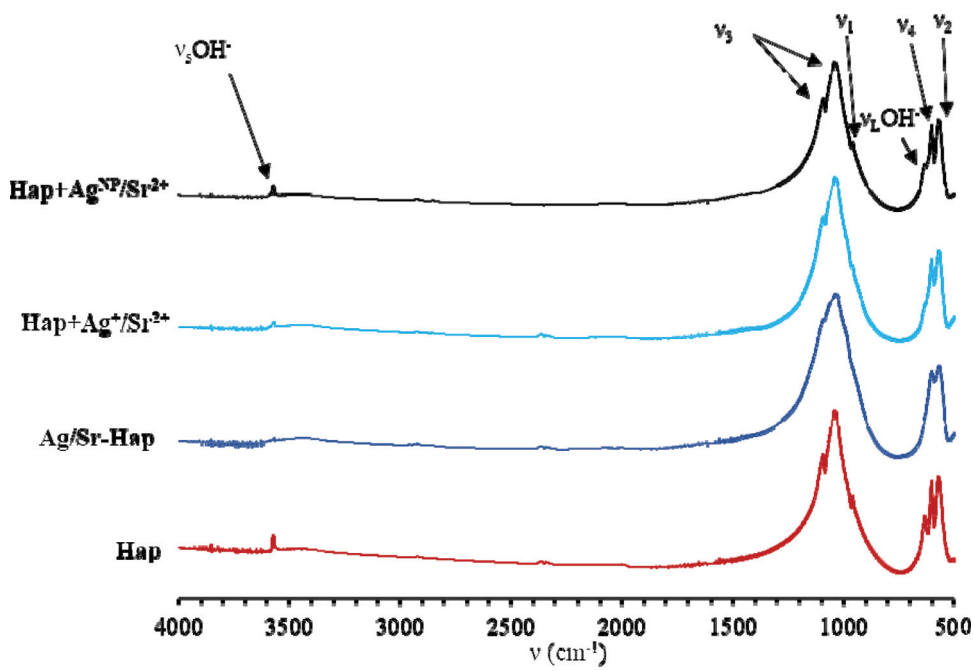


Fig. 3. FTIR spectra of the coatings, with phosphate  $\text{PO}_4^{3-}$  bands represented with the  $\nu_1$ ,  $\nu_2$ ,  $\nu_3$  and  $\nu_4$  signs and  $\text{OH}^-$  bands represented with  $\nu_5\text{OH}^-$  and  $\nu_1\text{OH}^-$ .

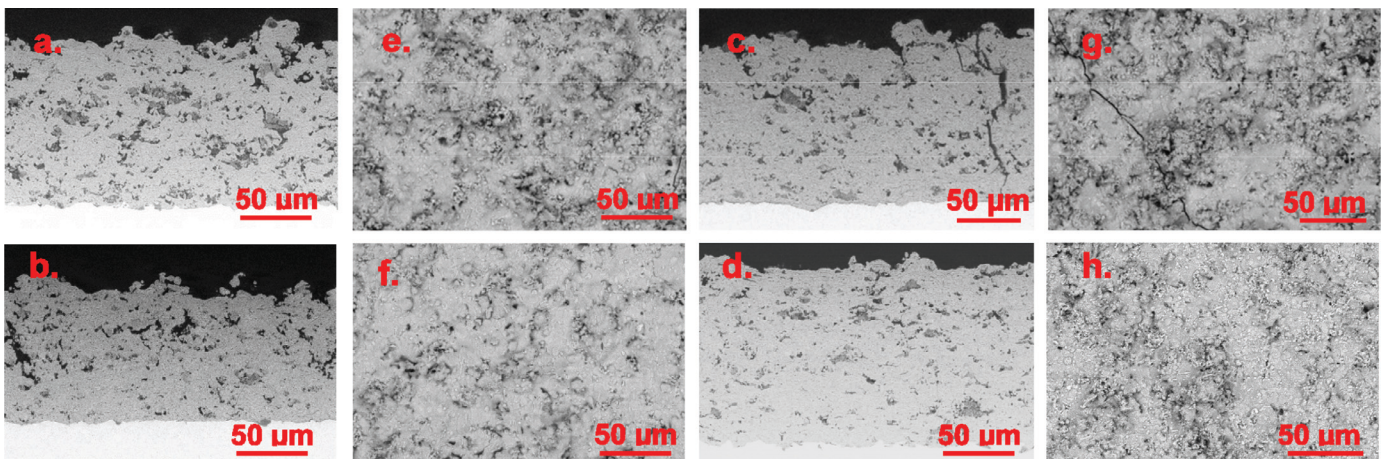


Fig. 4. SEM images of respectively cross sections and top surfaces of Hap (a, e), Ag/Sr-Hap (b, f), Hap +  $[\text{Ag}^+]/[\text{Sr}^{2+}]$  (c, g), Hap +  $\text{Ag}^{\text{NP}} + [\text{Sr}^{2+}]$  (d, h) coatings at x500 magnification.

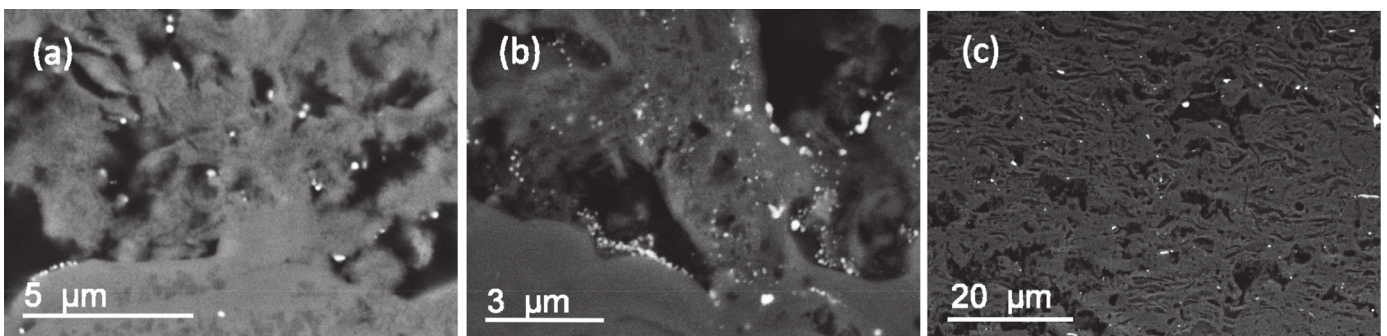


Fig. 5. SEM images of silver particles in Ag/Sr-Hap coating (a), Hap +  $[\text{Ag}^+]/[\text{Sr}^{2+}]$  (b) and Hap +  $\text{Ag}^{\text{NP}} + [\text{Sr}^{2+}]$ , in white.



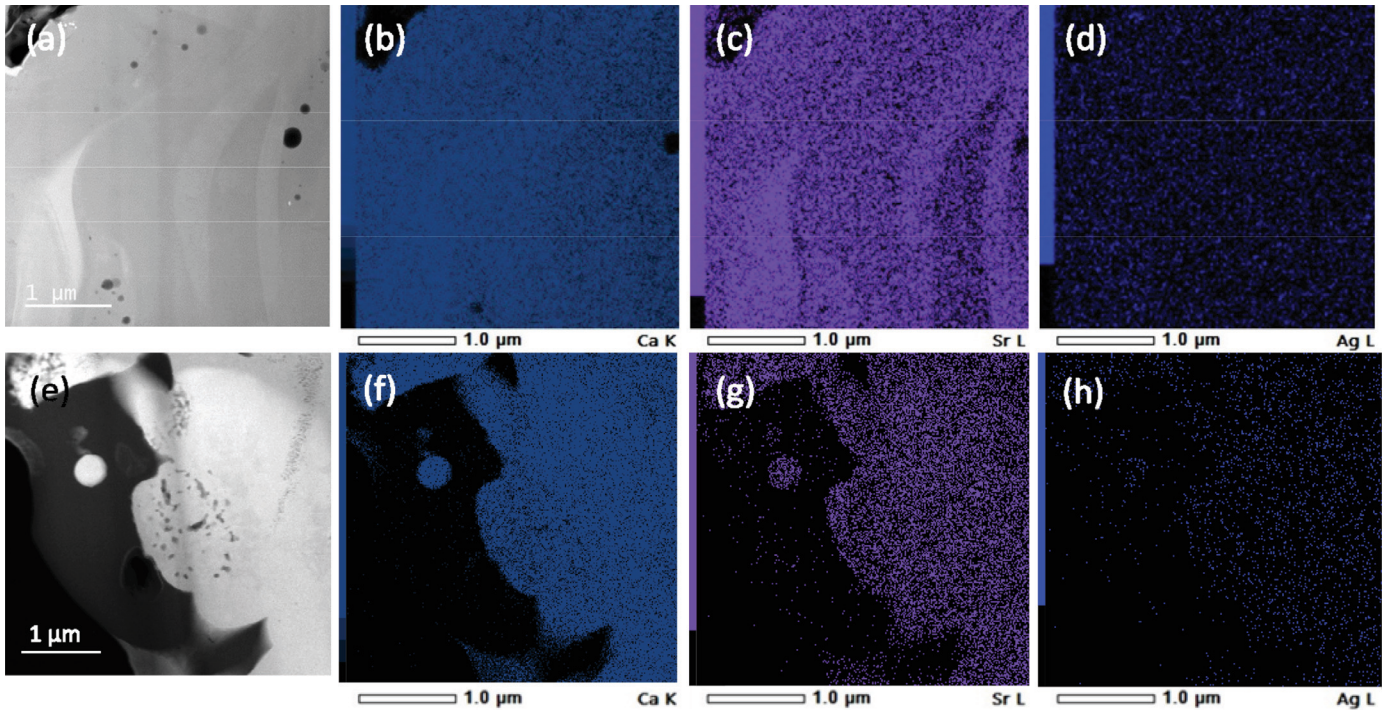


Fig. 6. STEM micrograph of Hap+[Ag<sup>+</sup>]/[Sr<sup>2+</sup>] (a) and Ag/Sr-Hap (e) coating cross-section and respective EDS mapping of Ca (b-f), Sr (c-g) and Ag (d-h).

**Table 3**  
Physical and elemental characteristics of coatings.

	Sa (μm)	Porosity (%)	wt.% Ag	wt.% Sr	(Ca+Sr) / P	Ø Ag np. (nm)	Contact angle (°)
Hap	5.4 ± 0.4	6.7 ± 3.1	0	0	-	0	18 ± 4
Ag/Sr-Hap	5.4 ± 0.3	5.0 ± 2.3	0.394 ± 0.004	4.62 ± 0.07	1.69 ± 0.02	231 ± 95	22 ± 13
Hap+Ag <sup>NP</sup> + [Sr <sup>2+</sup> ]	4.4 ± 0.1	3.0 ± 1.5	0.064 ± 0.002	4.23 ± 0.08	1.79 ± 0.02	810 ± 646	39 ± 12
Hap+[Ag <sup>+</sup> ]/[Sr <sup>2+</sup> ]	4.4 ± 0.1	2.5 ± 1.6	0.342 ± 0.005	4.55 ± 0.06	1.80 ± 0.02	115 ± 91	48 ± 7

**Table 4**  
Mechanical and biological properties of coatings.

	Adhesion energy (mJ)	Residual coating proportion (%)	Cell viability CV after 14 days (%)	Antibacterial reduction BR at 24 h (%)
APS Reference	0.9 ± 0.1	93 ± 3	100	-
Hap	4.2 ± 1.1	22 ± 3	105.4	-
Ag/Sr-Hap	5.5 ± 2.9	91 ± 13	99.42	2.9 ± 1.2
Hap+Ag <sup>NP</sup> + [Sr <sup>2+</sup> ]	7.6 ± 4.2	79 ± 2	38.06	1.2 ± 0.9
Hap+[Ag <sup>+</sup> ]/[Sr <sup>2+</sup> ]	4.3 ± 1.9	61 ± 2	99.97	5.0 ± 1.2

lution of Ag/Sr-Hap coating has released about 4.5 times more strontium and 1.5 times more calcium compared with the coating elaborated from Hap+[Ag<sup>+</sup>]/[Sr<sup>2+</sup>]. The proportion of Sr<sup>2+</sup> averages 5 at.% of the cations (Ca<sup>2+</sup>, Sr<sup>2+</sup> and Ag<sup>+</sup>) in the Ag/Sr-Hap and Hap+[Ag<sup>+</sup>]/[Sr<sup>2+</sup>] coatings. But this ratio reaches 24 at.% and 9.4 at.% in the dissolution medium for Ag/Sr-Hap and Hap+[Ag<sup>+</sup>]/[Sr<sup>2+</sup>] respectively, which means that strontium is preferentially released in the case of the coating made from the doped powder. As Ag/Sr-Hap has a low crystallinity and a high proportion of secondary phases evidenced by XRD and FTIR analyses, it can be assumed that strontium is likely incorporated in the secondary phases. This conclusion is reinforced by the fact that these phases are known to be more soluble than hydroxyapatite in a biological medium. Some studies also suggest a preferential incorporation, at

high concentration, of strontium into the TCP structure [36,37], that is a crystalline phase present in quite high proportion in the Ag/Sr-Hap coating. Finally, X-ray diffractograms of the coating surfaces recorded after dissolution that revealed the disappearance of the secondary phases for all the coatings, tend to confirm this interpretation. The pH evolution curves of the medium in contact with the doped samples show the same trend with an initial burst followed by a significant decrease during the first 500 min, followed by a re-increase and a stabilization at an intermediate level after 2000 min. The end values differ, with 6.07 for the annealed sample, 6.85 for Hap+[Ag<sup>+</sup>]/[Sr<sup>2+</sup>] and 7.02 for Ag/Sr-Hap. The kinetic of release of Ag in the medium is very different from the ones of strontium or calcium and can be compared with the pH evolution curve. Silver strongly dissolves when the pH is the lowest, and as

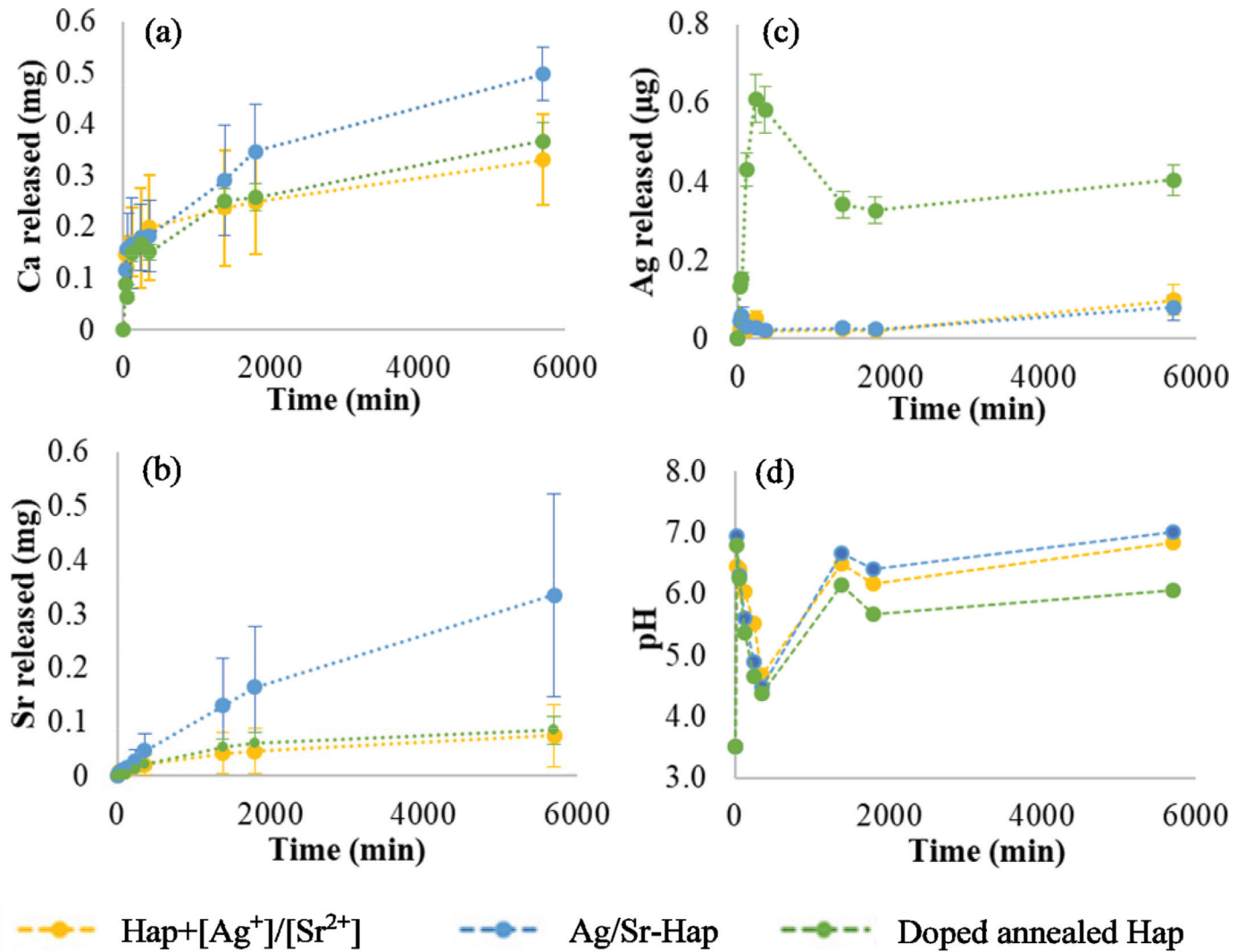


Fig. 7. Released cumulated quantity of calcium (a), strontium (b) and silver (c) in the doped coating and pH evolution with time (d).

pH starts rising due to the dissolution of the phosphocalcic matrix, it stops dissolving and seems to precipitate, as highlighted by both curves (Fig. 7c and 7d).

### 3.3. Mechanical properties

The results of the 3-point bending test applied on the samples were evaluated in comparison with the commercial APS plasma-sprayed hydroxyapatite coating (Table 4). All rf-SPS coatings show adhesion energies 4.6 to 8.4 times better than the one (0.9 mJ) of the commercial coating, with the max value (7.6 mJ) measured for Hap+Ag<sup>NP</sup>+Sr<sup>2+</sup> coating. No specific trend can be drawn except that the standard deviation increases with the value itself. Commercial coating as well as Ag/Sr-Hap and Hap+Ag<sup>NP</sup>+Sr<sup>2+</sup> coatings exhibited a cohesive rupture (over 60% of the coating is still attached to the substrate after the test). For Hap+Ag<sup>+</sup>/Sr<sup>2+</sup> a mixed mode (61%) rupture was identified and for the undoped coating Hap it was an adhesive (22%) rupture. No direct correlation between the adherence energy values and the failure dynamics were established.

### 3.4. In vitro cell-materials interaction

Cell proliferation results on the samples after 4, 7 and 14 days of incubation are shown in Fig. 8, Tab IV. At each time interval, the number

of cells on undoped (Hap and Reference) coatings and doped (Ag/Sr-Hap and Hap+[Ag<sup>+</sup>]/[Sr<sup>2+</sup>]) coatings was quite identical and considerably greater than that on Hap+Ag<sup>NP</sup>+Sr<sup>2+</sup> coating. The proliferation rates reached more than 500% of their initial population after 14 days, with a slightly better result for Hap coating than for the reference. At day 7, Hap+[Ag<sup>+</sup>]/[Sr<sup>2+</sup>] showed a promising burst (340%) since it overtook both undoped coatings (290%), but this result was not confirmed at 14 days. The addition of silver as nanoparticles in the suspension had a significant negative impact on cell proliferation, diminishing the cell viability below 70%.

### 3.5. Antimicrobial activity

Bactericidal potential of our coatings toward *S. aureus* was explored, and different behaviours emerged depending on the doping route (Fig. 9). The undoped coatings (Reference and Hap), as anticipated, did not show any antibacterial effectiveness and no significant difference could be detected between them, implying that the change of microstructural scale does not impact the bacterial growth. If Ag/Sr-Hap gave troubling results after 6 h with a significant proliferation of bacteria, it finally met the antibacterial expectations with a reduction BR of 2.9 after 24 h (Table 4). Hap+[Ag<sup>+</sup>]/[Sr<sup>2+</sup>] coating proved itself very efficient since it reduced the number of viable cells by almost 5 log after 24 h of inoculation. On the other hand, Hap+Ag<sup>NP</sup>+Sr<sup>2+</sup> coating

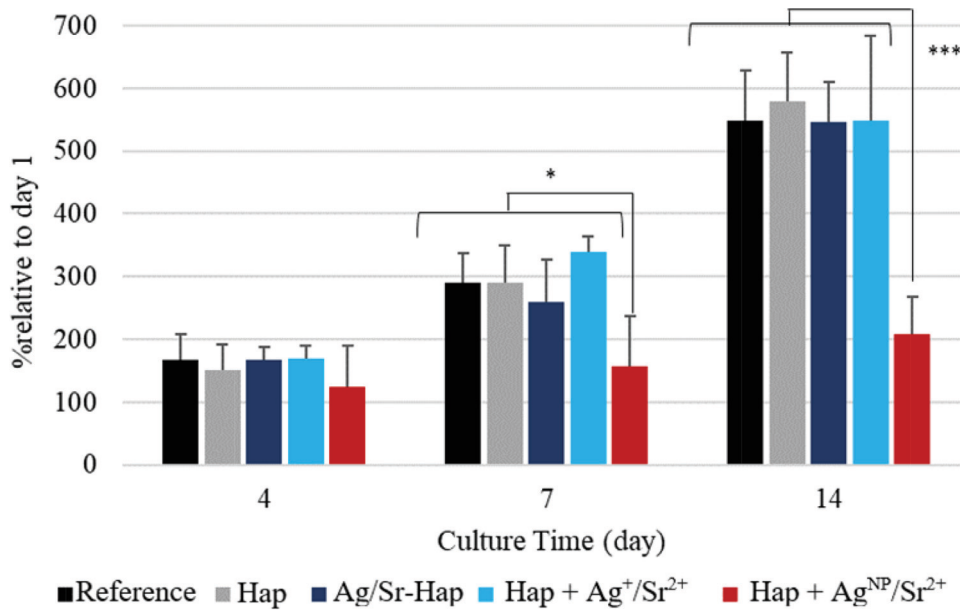


Fig. 8. Proliferation of hMSC with time on plasma-sprayed coatings ( $n = 5$ ), \*  $P \leq 0.05$  \*\*\*  $P \leq 0.001$ .

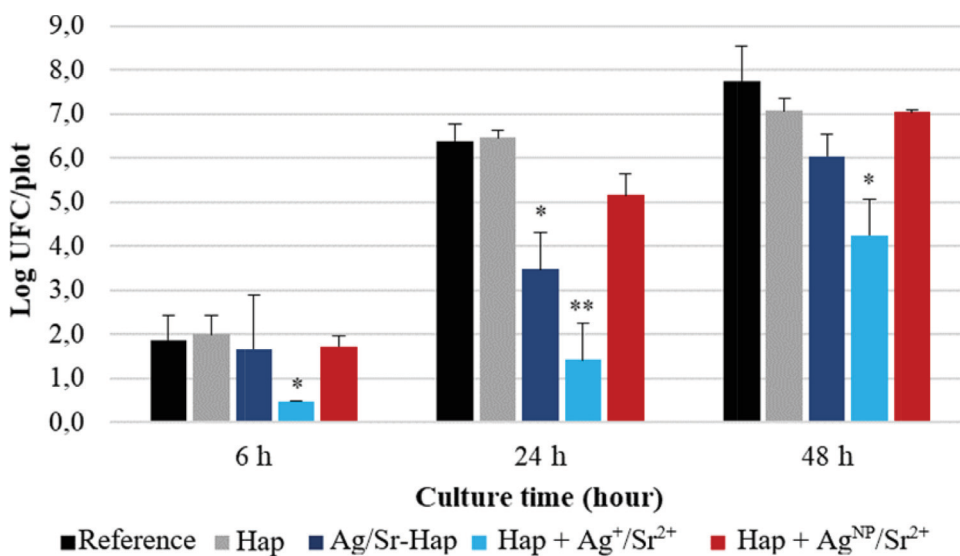


Fig. 9. Bacterial proliferation of *S. aureus* on doped and undoped coatings ( $n = 3$ ), \*  $P \leq 0.05$  \*\*  $P \leq 0.01$ .

showed a reduction  $BR$  of 1.2 only, which is insufficient from a bactericidal point of view.

#### 4. Discussion

##### 4.1. Influence of the suspension formulation on the coating composition

The chemical stability of hydroxyapatite coatings in a biological medium is essential to guarantee their sustainability. Among the characteristics intimately related to this stability, the crystallinity and the phase purity of the coating are predominant since they determine both its resorbability and its mechanical properties, and those characteristics are mainly determined by the spraying conditions. The decomposition of stoichiometric hydroxyapatite and the formation of secondary including amorphous phases are a common occurrence in conventional plasma spray. The high temperature of the plasma arc and the rapid cooling at the substrate impact lead to the formation of decomposition phases (TCP, TTCP, ACP and CaO), which weaken the coating by re-

sorbing significantly faster in the body than hydroxyapatite [38,39]. Consequently, the ISO 13 779: 2018 standard requires a percentage of the secondary phases lower than 30 wt.%, and a coating with a crystallinity ratio greater than 45%. The X-ray diffractometry data shown in Fig. 2 and Table 2 indicate that coatings made with a suspension containing the doping elements as nitrates are constituted of TTCP and CaO as secondary phases in contrast to the equivalent undoped Hap coating that contains  $\alpha$ -TCP, TTCP and CaO for a similar concentration of hydroxyapatite. In suspension plasma spraying, the disturbance caused by the addition of substances such as nitrates or metal nanoparticles in the dispersive medium modifies the plasma thermal characteristics and therefore the heat treatment sustained by phosphocalcic particles. Their degree of decomposition can thus be largely affected: in the present case, nitrates increase the thermal flux available leading to high temperature phase formation while maintaining high crystallinity ratio and HA% as compared to undoped coating (Hap). Regarding the microstructure, parameters such as the porosity and the roughness also seem to be impacted: the presence of nitrates and the use of a non-stoichiometric doped pow-

der lead to a decrease of porosity, due to a higher melting degree in the former case, and to a lack of crystallinity which favors the compacity of the matter at impact in the latter case. Research has shown that HA is an ideal platform for cationic substitution and, specifically, silver and strontium ions can substitute calcium ion in the apatite structure. As the addition of such dopants can alter the physico-chemical characteristics of HA, one would have expected peak shifts in the XRD analysis of the coatings indicating significant incorporation of the doping ions in the HA lattice structure due to the use of either the doped powder (Ag/Sr-Hap) or the doped medium (Hap+Ag<sup>NP</sup>+ [Sr<sup>2+</sup>] or Hap+[Ag<sup>+</sup>]/[Sr<sup>2+</sup>]). While no peak shifts were observed for doped coatings, it remains likely that Sr was incorporated in one of the calcium phosphate lattice structure as no separate Sr or SrO peaks were detected in the diffractograms. In contrast, identification of Ag or Ag<sub>2</sub>O peaks in the diffractograms and the observation of the coating microstructure evidenced that silver is not incorporated in the HA lattice structure. High magnification SEM and STEM observations clearly confirmed that silver is incorporated as nanoparticles in the doped coatings, whose sizes depend on the doping method. Indeed, its ionic radius 14% higher than that of calcium (128 ppm versus 112 ppm respectively for a coordination number CN = 8, [40, 41]) combined with the charge mismatch reveal the instability of the Ag<sup>+</sup> ion into the apatite structure, either preventing its incorporation during spraying or leading to its migration out of the apatitic structure, which probably induces the significant drop of crystallinity noticed for Ag/Sr-Hap coating. Due to this phenomenon, a large amount of silver dopant is lost during spraying (mainly because of the temperature and pressure that favor volatilization of metallic silver) and the exact amount present into the coating is hardly controllable. To confirm the chemical state of silver in Hap+Ag<sup>NP</sup>+ [Sr<sup>2+</sup>] and Hap+[Ag<sup>+</sup>]/[Sr<sup>2+</sup>] coatings, XPS analysis was performed on coatings with a 10 times higher silver concentration in order to detect silver and deconvolute the doublet 3d<sub>3/2</sub> et 3d<sub>5/2</sub> (367,75 eV for 3d<sub>5/2</sub> et 373,75 eV pour 3d<sub>3/2</sub>). It showed that silver nanoparticles in the Hap+[Ag<sup>+</sup>]/[Sr<sup>2+</sup>] coating are 90% metallic and 10% oxidized, while they are 65% metallic and 35% oxidized in the Hap+Ag<sup>NP</sup>+ [Sr<sup>2+</sup>] coating. According to the Ellingham's diagram, for a partial oxygen pressure of 0.062 bar, silver oxide is reduced to metallic silver at a temperature above 398 K (approximately 125 °C). During plasma-spraying, most particles reach much higher temperatures on the probe-substrate path. But out of thermodynamic equilibrium, the thermal energy transmitted to reduce the silver oxide to metallic silver is limited by dynamic consideration, due to short residence time of the droplets/particles. For suspensions containing Ag<sup>NP</sup> silver nanoparticles and considering that these nanoparticles are already partly oxidized before plasma-spraying, their conversion to fully metallic nanoparticles is further limited because of their lower surface/volume ratio which does not favor the thermal transfer. For the doping mode involving Ag<sup>+</sup> ions, and taking into account the instability of silver oxide over metallic silver in the spraying conditions, it can be assumed that most of the ions are instantly reduced in metallic silver either without going through an oxidized state, or undergoing a more extensive reduction of oxidized particles due to their smaller size. Because the silver peak was too weak to perform a quality deconvolution of the XPS spectrum recorded for Ag/Sr-Hap coating, and since the concentration of silver could not be sufficiently increased in the Ag/Sr-Hap precursor powder, the chemical state of the silver particles could not be evaluated. Thanks to the elemental analysis performed by STEM (Fig. 6), it was clearly established that strontium is homogeneously incorporated in the calcium phosphate lattice structure regardless of its ionic radius (126 ppm), even though some splats of doped coatings produced from nitrates revealed concentration heterogeneities with strontium-richer zones located at the grain boundaries of the splats. From the elemental point of view, the (Ca+Sr)/P (Table 3) ratios of Hap+Ag<sup>NP</sup>+ [Sr<sup>2+</sup>] and Hap+[Ag<sup>+</sup>]/[Sr<sup>2+</sup>] are the highest of all (1.79 ± 0.02 and 1.80 ± 0.02 respectively against 1.73 ± 0.03 for the undoped coating), validating Sr incorporation or phosphorus evaporation during plasma spraying. Since Ag left the ap-

atitic structure during plasma spraying, it was not included in the ratio.

#### 4.2. Microstructure and mechanical properties

The coating bond strength is as crucial as its chemistry for the clinical success of load bearing implants. The adhesion energy (Table 4) that was determined in the present study represents the force required to detach the coating from the substrate. Depending on the failure mode, the adhesion energy reflects the tenacity either of the interface, either of the nearby microstructure. For the undoped SPS coating (Hap) the percentage of residual coating only reaches 22%, corresponding to an adhesive failure, while for the APS reference it is about 93%, corresponding to a cohesive failure. A cohesive type failure (residual coating > 60%) means that the cohesion of the microstructure near the interface is weaker than the coating/substrate interface. Indeed, it is generally the most fragile area because of the higher proportion of amorphous phases, due to a lower local crystallization of the material caused by quenching. This localized amorphization has a double effect on the adhesion energy: on one hand it promotes the anchoring of the coating by limiting the generation of residual stresses usually generated by the crystallization of the material, but on the other hand it weakens the cohesion of the phosphocalcic material itself [42]. These two antagonistic effects therefore contribute to define the failure mode and adhesion energy. The evolution of the crystallinity ratio with the failure mode and the adhesion energy is illustrated in Fig. 10. Therefore, for a low crystallinity ratio of the coating (Ag/Sr-Hap) the rupture is typically cohesive, while for a high ratio (undoped Hap), the rupture is adhesive. In the case of the undoped coating, since it broke at a lower adhesion energy than the doped Ag/Sr-Hap coating, it could be assumed that there is a higher amount of residual stresses at its interface, certainly caused by the high stability of undoped hydroxyapatite that favors a faster crystallization. When using nitrates in the precursor suspension (Hap+[Ag<sup>+</sup>]/[Sr<sup>2+</sup>] and Hap+Ag<sup>NP</sup>+Sr<sup>2+</sup>), the crystallinity ratios are similar to that of the undoped coating (67 and 70%), but the amount of high temperature secondary phases (TTCP and CaO) is higher, which makes the rupture evolve from adhesive towards the mixed and cohesive type (61% and 79% residual coating respectively). It is certainly the high melting degree of the phosphocalcic particles caused by the use of nitrates that explains the improvement of the surface of contact with the substrate, providing a stronger interface. However, it was found that the adhesion energy is much higher for Hap+Ag<sup>NP</sup>+Sr<sup>2+</sup> (7.6 ± 4.2 mJ) than for Hap+[Ag<sup>+</sup>]/[Sr<sup>2+</sup>] (4.3 ± 1.9 mJ). Since its failure mode is more adhesive, the decrease of the adhesion energy for Hap+[Ag<sup>+</sup>]/[Sr<sup>2+</sup>] can be attributed to a weakening of the anchoring of the deposit. It is noteworthy to mention that the only distinguishing characteristics between these two coatings are the concentration and the size of the silver nanoparticles. It is therefore assumed that the higher proportion and the finer size of the nanoparticles resulting from the silver nitrates both reduce the contact surface and thus anchorage of the coating. The Ag/Sr-Hap and Hap+[Ag<sup>+</sup>]/[Sr<sup>2+</sup>] coatings exhibit the same silver concentrations, shape, and dispersion of the silver nanoparticles as well as strontium concentrations, but their crystallinity ratios are far apart. Ag/Sr-Hap is the least crystalline of all coatings, justifying why its interface is stronger and why the failure mode is cohesive.

#### 4.3. Physicochemical properties and biological behavior

Regarding the effect of doping on cell proliferation, it seems that cells proliferate preferentially on the undoped coatings (578% for Hap and 549% for Reference at day 14). Among the doped substances, Hap+[Ag<sup>+</sup>]/[Sr<sup>2+</sup>] and Ag/Sr-Hap coatings are the most favorable (549 and 546% respectively), while the Hap+Ag<sup>NP</sup>+ [Sr<sup>2+</sup>] coating shows an intermediate behavior (209%). As a value of cell viability below 70% reports a potential cytotoxic material, this coating does not meet the

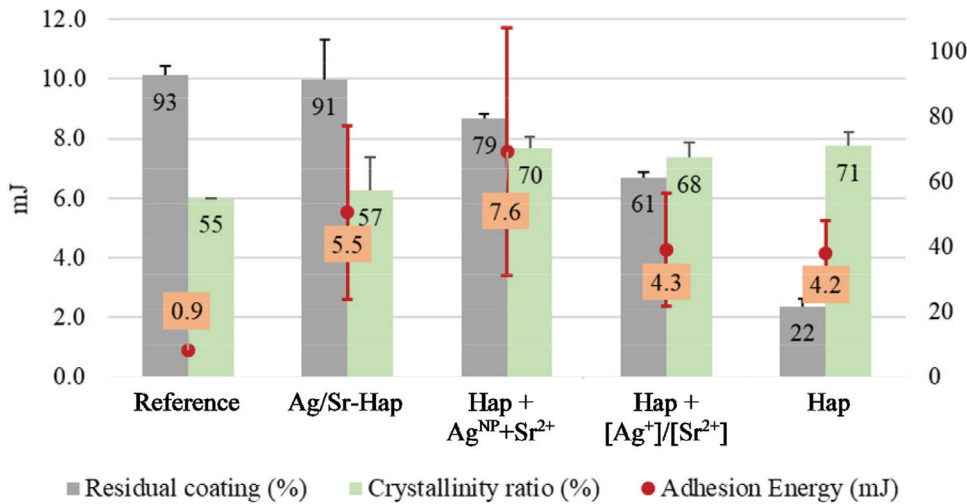


Fig. 10. Evolution of the mechanical properties of the coatings with the crystallinity ratio  $R_1$ .

requirements. This means that the cells proliferate more favorably on the surfaces where silver nanoparticles sizes are small and uniformly distributed than on those with larger agglomerates, with little effect of the silver content. Work conducted by Albers et al. [10] states that silver harmfulness is mainly carried by the  $\text{Ag}^+$  ions. In addition, it has been shown in other studies that the chemical stability of the coating influences cell proliferation [43]. This is also possibly the case with silver, especially since its dissolution depends on the pH of the medium, which in turn depends on the amount of  $\text{OH}^-$  and  $\text{PO}_4^{3-}$  ions released from the phosphocalcic matrix. Indeed, silver is further dissolved when the phosphocalcic matrix is poorly soluble because the pH is maintained longer at low values at the periphery of the surface, as demonstrated with the annealed doped sample. This coating releases less calcium, strontium, phosphate and hydroxyl ions than the others because of its high crystallinity and hydroxyapatite proportion. But it releases significantly more silver even though the initial Ag concentration of the deposit is similar ( $0.313 \pm 0.007$  wt.%). Crystalline state thus first determines the solubility degree of the coating, solubility that can be increased by a large exchange surface with the medium, defined by roughness and porosity. As evidenced during the dissolution test, the solubility of doped coatings evolves in the following order:  $\text{Ag/Sr-Hap} > \text{Hap} + [\text{Ag}^+]/[\text{Sr}^{2+}] (\approx \text{Hap} + \text{Ag}^{\text{NP}} + [\text{Sr}^{2+}])$ . This explains why Ag/Sr-Hap coating does not block cell proliferation: its low crystallinity (57%) combined with a relatively high porosity (5%) is favorable to the dissolution of its matrix and to the increase of pH, so that it releases only very few  $\text{Ag}^+$  ions. But when the CaP matrix dissolves quickly, silver nanoparticles do not, gradually concentrating them at the surface. The fact that cellular proliferation is not compromised means cells are more sensitive to  $\text{Ag}^+$  flux than to Ag nanoparticles, confirming the results of Albers et al. [10]. For the  $\text{Hap} + [\text{Ag}^+]/[\text{Sr}^{2+}]$  coating, the solubility of which is intermediate, the release of  $\text{Ag}^+$  ions is a little more pronounced, but the nanoparticles of homogeneous and fine grain size distribution release  $\text{Ag}^+$  ions in a sufficiently diluted concentration not to alert the cells. On the other hand, at equal phosphocalcic matrix dissolution and because of the large size of the silver nanoparticles despite their low concentration, the  $\text{Ag}^+$  ion fluxes coming from the surface of  $\text{Hap} + \text{Ag}^{\text{NP}} + [\text{Sr}^{2+}]$  are locally important, alerting the cells and blocking their division. The antibacterial efficacy  $BR$  is high for the  $\text{Hap} + [\text{Ag}^+]/[\text{Sr}^{2+}]$  sample (5.0 at 24 h), due to its high silver level (0.342 wt.%) and favored  $\text{Ag}^+$  ion release. Ag/Sr-Hap coating has a  $BR$  of 2.9 with a similar silver concentration (0.394 wt.%) but, because of the high solubility of the matrix, its release is slower. The fact that  $\text{Hap} + [\text{Ag}^+]/[\text{Sr}^{2+}]$  has a higher efficiency than Ag/Sr-Hap suggests a stronger effect of the  $\text{Ag}^+$  ions on bacteria in comparison with the metallic Ag(s) particles present on the surface. Finally,  $\text{Hap} + \text{Ag}^{\text{NP}} + [\text{Sr}^{2+}]$  sample has the lowest value of  $BR$

(1.2), probably due to its silver concentration that is 5 to 6 times lower than the previous ones.

## 5. Conclusions

In this study, three silver and strontium-doped hydroxyapatite coatings were synthesized by rf-SPS, implementing suspensions containing strontium in its ionic state (free or incorporated in the Hap powder) and silver under metallic or ionic state and dispersed either in the powder precursor or in the liquid medium. Strontium and silver were chosen in order to promote mesenchymal cell proliferation while disabling the development of *S. aureus* resistant bacteria. Suspension plasma spraying provides access to a versatility that conventional plasma spraying lacks. By changing the formulation of the precursor as by the addition of nitrates or metal nanoparticles in the dispersing medium, one can directly influence characteristics such as porosity, crystallinity or composition. Some biological properties as the antibacterial efficiency seems to be mainly driven by the silver content and the release extent of the silver ions, while the hMSC affinity for the surface seems rather linked to the chemical stability of the phosphocalcic matrix and the size of the silver nanoparticles. The  $\text{Hap} + [\text{Ag}^+]/[\text{Sr}^{2+}]$  coating is the one that combines very good mechanical properties compared to the APS reference coating, excellent affinities for cells, and bactericidal activity. It has also compliant physicochemical properties (crystalline composition, porosity), and a potential good chemical stability. By incorporating the dopants in ionic form in the precursor, the fine and homogeneous dispersion of the dopants at the micrometric scale within the apatite structure is guaranteed and does not compromise the mechanical or biological properties of the phosphocalcic matrix. This study thus demonstrates the potential of the rf-SPS technique for the development of nanostructured-hydroxyapatite coatings with controlled antibacterial and anti-inflammatory doping.

## Declaration of Competing Interest

The authors declare that they have no known competing financial interests or personal relationships that could have appeared to influence the work reported in this paper.

## Acknowledgements

This work was supported by the Agence Nationale de la Recherche of France under project named ARCHICAP (ANR-15-CE19-0021) and the Région Occitanie in France under project named REVAMITIC (CLE).

## References

- [1] ANSM, Etude des facteurs associés aux révisions sur prothèses totales de hanche (PTH) : rôle du mode d'ancrage (cimentage) et des constituants prothétiques (couple de frottement) dans les révisions chirurgicales, 2015.
- [2] Haute Autorité de Santé, Prothèse de hanche ou de genou : diagnostic et prise en charge de l'infection dans le mois suivant l'implantation, (2014) 1–134.
- [3] G.A. Fielding, M. Roy, A. Bandyopadhyay, S. Bose, Antibacterial and biological characteristics of silver containing and strontium doped plasma sprayed hydroxyapatite coatings, *Acta Biomater.* 8 (2012) 3144–3152, doi:10.1016/j.actbio.2012.04.004.
- [4] Z. Geng, Z. Cui, Z. Li, S. Zhu, Y. Liang, Y. Liu, X. Li, X. He, X. Yu, R. Wang, X. Yang, Strontium incorporation to optimize the antibacterial and biological characteristics of silver-substituted hydroxyapatite coating, *Mater. Sci. Eng. C* 58 (2016) 467–477, doi:10.1016/j.msec.2015.08.061.
- [5] Elliott, *Structure and Chemistry of the Apatites and Other*, Elsevier, 1994.
- [6] J. Kolmas, E. Groszyk, D. Kwiatkowska-Rózycka, Substituted hydroxyapatites with antibacterial properties, *Biomed. Res. Int.* (2014) 2014, doi:10.1155/2014/178123.
- [7] S. Eto, S. Kawano, S. Someya, H. Miyamoto, M. Sonohata, M. Mawatari, First Clinical Experience With Thermal-Sprayed Silver Oxide-Containing Hydroxyapatite Coating Implant, *J. Arthroplasty.* 31 (2016) 1498–1503, doi:10.1016/j.arth.2015.12.034.
- [8] M. Trop, M. Novak, S. Rodl, B. Hellbom, W. Kroell, W. Goessler, Silver-coated dressing acticoat caused raised liver enzymes and argyria-like symptoms in burn patient, *J. Trauma Inj. Infect. Crit. Care* 60 (2006) 648–652, doi:10.1097/01.ta.0000208126.22089.b6.
- [9] M.A. Hollinger, Toxicological aspects of topical silver pharmaceuticals, *Crit. Rev. Toxicol.* 26 (1996) 255–260, doi:10.3109/10408449609012524.
- [10] C.E. Albers, W. Hofstetter, K.A. Siebenrock, R. Landmann, F.M. Klenke, In vitro cytotoxicity of silver nanoparticles on osteoblasts and osteoclasts at antibacterial concentrations, *Nanotoxicology* 7 (2013) 30–36, doi:10.3109/17435390.2011.626538.
- [11] M. Šupová, Substituted hydroxyapatites for biomedical applications: a review, *Ceram. Int.* 41 (2015) 9203–9231, doi:10.1016/j.ceramint.2015.03.316.
- [12] E.S. Thian, P.N. Lim, Z. Shi, B.Y. Tay, K.G. Neoh, Silver-doped apatite as a bioactive and an antimicrobial bone material, *Key Eng. Mater.* 493–494 (2012) 27–30 doi:10.4028/www.scientific.net/KEM.493-494.27.
- [13] C. Capuccini, P. Torricelli, F. Sima, E. Boanini, C. Ristoscu, B. Bracci, G. Socol, Strontium-substituted hydroxyapatite coatings synthesized by pulsed-laser deposition : in vitro osteoblast and osteoclast response, *Acta Biomater.* 4 (2008) 1885–1893, doi:10.1016/j.actbio.2008.05.005.
- [14] C. Lindahl, S. Pujari-Palmer, A. Hoess, M. Ott, H. Engqvist, W. Xia, The influence of Sr content in calcium phosphate coatings, *Mater. Sci. Eng. C* 53 (2015) 322–330, doi:10.1016/j.msec.2015.04.015.
- [15] D.S. Brauer, N. Karpukhina, G. Kedia, A. Bhat, R.V. Law, I. Radecka, R.G. Hill, D.S. Brauer, Bactericidal strontium-releasing injectable bone cements based on bioactive glasses, *J. R. Soc. Interface* (2012) 1–8, doi:10.1098/rsif.2012.0647.
- [16] J.T.B. Ratnayake, M. Mucalo, G.J. Dias, Substituted hydroxyapatites for bone regeneration : a review of current trends, *J. Biomed. Mater. Res. Part B* (2017) 1285–1299, doi:10.1002/jbm.b.33651.
- [17] H. Qiao, G. Song, Y. Huang, H. Yang, S. Han, Si, Sr, Ag co-doped hydroxyapatite/TiO<sub>2</sub> coating: enhancement of its antibacterial activity and osteoinductivity, *RSC Adv.* 9 (2019) 13348–13364, doi:10.1039/c9ra01168d.
- [18] Y. Huang, X. Zhang, H. Zhang, H. Qiao, X. Zhang, T. Jia, S. Han, Y. Gao, H. Xiao, H. Yang, Fabrication of silver- and strontium-doped hydroxyapatite/TiO<sub>2</sub> nanotube bilayer coatings for enhancing bactericidal effect and osteoinductivity, *Ceram. Int.* 43 (2016) 992–1007, doi:10.1016/j.ceramint.2016.10.031.
- [19] International standard ISO\_13779, Implants for surgery — Hydroxyapatite - Part 2: Coatings of Hydroxyapatite, (2008).
- [20] International standard ISO\_13779, Implants for surgery — Hydroxyapatite - Part 3: Chemical Analysis and Characterization of Crystallinity and Phase Purity, (2008).
- [21] T.J. Webster, C. Ergun, R.H. Doremus, R.W. Siegel, R. Bizios, Enhanced functions of osteoblasts on nanophase ceramics, *Biomaterials* 21 (2000) 1803–1810.
- [22] M. Roy, A. Bandyopadhyay, S. Bose, Induction plasma sprayed Sr and Mg doped nano hydroxyapatite coatings on Ti for bone implant, *J. Biomed. Mater. Res. Part B Appl. Biomater.* 99 (2011) 258–265 B, doi:10.1002/jbm.b.31893.
- [23] M. Roy, G.A. Fielding, H. Beyenal, A. Bandyopadhyay, S. Bose, Mechanical, in vitro antimicrobial, and biological properties of plasma-sprayed silver-doped hydroxyapatite coating, *ACS Appl. Mater. Interfaces* 4 (2012) 1341–1349, doi:10.1021/am201610q.
- [24] P. Fauchais, Suspension and solution plasma spraying, *J. Phys. D Appl. Phys.* 46 (2013) 14pp, doi:10.1088/0022-3727/46/22/224015.
- [25] S. Kannan, J.M.F. Ferreira, Synthesis and thermal stability of hydroxyapatite- $\beta$ -tricalcium phosphate composites with cosubstituted sodium, magnesium, and fluorine, *Chem. Mater.* 18 (2006) 198–203, doi:10.1021/cm051966i.
- [26] P. Ducheyne, *Comprehensive Materials*, Elsevier Science, 2011.
- [27] R.B. Heimann, Plasma-sprayed hydroxylapatite-based coatings: chemical, mechanical, microstructural, and biomedical properties, *J. Therm. Spray Technol.* 25 (2016) 827–850, doi:10.1007/s11666-016-0421-9.
- [28] M. Roy, A. Bandyopadhyay, S. Bose, Induction plasma sprayed nano hydroxyapatite coatings on titanium for orthopaedic and dental implants, *Surf. Coatings Technol.* 205 (2011) 2785–2792, doi:10.1016/j.surfcoat.2010.10.042.
- [29] E. Bouyer, F. Gitzhofer, M.I. Boulos, Suspension plasma spraying for hydroxyapatite powder preparation by RF plasma, *IEEE Trans. Plasma Sci.* 25 (1997) 1066–1072, doi:10.1109/27.649627.
- [30] R. d'Haese, L. Pawlowski, M. Bigan, R. Jaworski, M. Martel, Phase evolution of hydroxapatite coatings suspension plasma sprayed using variable parameters in simulated body fluid, *Surf. Coatings Technol.* 204 (2010) 1236–1246, doi:10.1016/j.surfcoat.2009.10.022.
- [31] K. Geels, D.B. Fowler, W.-U. Kopp, M. Rückert, Material/Preparation Tables—Methods C-01/T-01 to C-68/T-68, in: *Metallographic and Materialographic Specimen Preparation, Light Microscopy, Image Analysis, and Hardness Testing*, 2006, pp. 223–226. <https://books.google.cl/books?id=oaehZy3Vo1kC>.
- [32] A.A. Roche, A.K. Behme, J.S. Solomon, A three-point flexure test configuration for improved sensitivity to metal, *J. Adhes. Adhes.* (1982) 249–254.
- [33] International standard ISO 14679:1997, Adhésifs - Détermination des caractéristiques d'adhésion par une méthode de flexion à trois points, (1997).
- [34] L. Berzina-Cimdina, N. Borodajenko, Research of calcium phosphates using fourier transform infrared spectroscopy, in: *Infrared Spectroscopy - Materials Science, Engineering and Technology*, 2012, pp. 123–148, doi:10.5772/36942.
- [35] W.K. Yeung, G.C. Reilly, A. Matthews, A. Yerokhin, In vitro biological response of plasma electrolytically oxidized and plasma-sprayed hydroxyapatite coatings on Ti-6Al-4V alloy, *J. Biomed. Mater. Res. Part B Appl. Biomater.* 101 (2013) 939–949 B, doi:10.1002/jbm.b.32899.
- [36] H.W. Kim, Y.H. Koh, Y.M. Kong, J.G. Kang, H.E. Kim, Strontium substituted calcium phosphate biphasic ceramics obtained by a powder precipitation method, *J. Mater. Sci. Mater. Med.* 15 (2004) 1129–1134, doi:10.1023/B:JMSM.0000046395.76435.60.
- [37] L. Leroux, J.L. Lacout, Preparation of calcium strontium hydroxyapatites by a new route involving calcium phosphate cements, *J. Mater. Res.* 16 (2001) 171–178, doi:10.1557/JMR.2001.0028.
- [38] C. Combes, C. Rey, *Biomatériaux à base de phosphates de calcium*, *Tech. l'ingénieur* (2013) 1–25 n4950.
- [39] S.V. Dorozhkin, Calcium orthophosphates – Occurrence, properties, biomineralization, pathological calcification and biomimetic applications, *Biomater* 1 (2) (2011) 121–164, doi:10.4161/biom.18790.
- [40] D.R. Lide, *Handbook of Chemistry and Physics*, 2004. doi:10.1016/0022-2860(92)85083-s.
- [41] A. Fihri, C. Len, R.S. Varma, A. Solhy, Hydroxyapatite: a review of syntheses, structure and applications in heterogeneous catalysis, *Coord. Chem. Rev.* 347 (2017) 48–76, doi:10.1016/j.ccr.2017.06.009.
- [42] G. Britain, *J. Metauforschung, Fracture mechanics studies of thermal mismatch using a four-point bending specimen*, *Acta Metall. Mater* 40 (1992) S345–S353.
- [43] G. Costa Machado, E. García-Tuñón, R.V. Bell, M. Alini, E. Saiz, M. Peroglio, Calcium phosphate substrates with emulsion-derived roughness: processing, characterisation and interaction with human mesenchymal stem cells, *J. Eur. Ceram. Soc.* 38 (2018) 949–961, doi:10.1016/j.jeurceramsoc.2017.06.043.